

JGR Space Physics

RESEARCH ARTICLE

10.1029/2024JA033610

Ionospheric *D* Region: Characteristics Near Dawn and Dusk

Neil R. Thomson¹ , Mark A. Clilverd² , and Craig J. Rodger¹ 

¹Physics Department, University of Otago, Dunedin, New Zealand, ²British Antarctic Survey (UKRI-NERC), Cambridge, UK

Key Points:

- “Wait” *D* region electron number density parameters, height H' and sharpness β , are determined through dawn and dusk for the first time
- At mid-latitudes H' shows a clear minimum at dawn consistent with the release of cosmic ray generated electrons accumulated overnight
- H' and β through dawn and dusk are a delicate balance between *D*-region ionization generated by solar EUV and galactic cosmic rays

Supporting Information:

Supporting Information may be found in the online version of this article.

Correspondence to:

M. A. Clilverd,
macl@bas.ac.uk

Citation:

Thomson, N. R., Clilverd, M. A., & Rodger, C. J. (2025). Ionospheric *D* region: Characteristics near dawn and dusk. *Journal of Geophysical Research: Space Physics*, 130, e2024JA033610. <https://doi.org/10.1029/2024JA033610>

Received 2 DEC 2024
Accepted 28 MAR 2025

©2025. The Author(s).

This is an open access article under the terms of the [Creative Commons Attribution License](https://creativecommons.org/licenses/by/4.0/), which permits use, distribution and reproduction in any medium, provided the original work is properly cited.

Abstract The characteristics of very low frequency (VLF) radio wave propagation in the Earth-ionosphere waveguide are determined particularly through dawn and dusk using phase and amplitude measurements of man-made signals propagating below the ionospheric *D* region. For the first time variations of “Wait” height and sharpness parameters, H' and β , have been determined for dawn and dusk conditions. These measurements provide observational data to constrain *D* region modeling efforts, extending the capabilities of VLF propagation monitoring for geophysical phenomena such as lightning, solar flares, and energetic particle precipitation. At mid-latitudes, H' varied from ~ 85 km at night, then, starting from solar zenith angle (SZA) $\sim -97.5^\circ$, rapidly down to ~ 73 km at dawn (SZA = -90°), then back up to ~ 78 km at SZA $\sim -75^\circ$ and then down to the appropriate noon value for the latitude (and season). In contrast, from noon through dusk to night, H' varied essentially monotonically from ~ 70 to 75 km through ~ 80 to ~ 85 km. At low latitudes no dawn minimum in H' was observed, due to the reduced effect of galactic cosmic rays (GCR). Sharpness, β , varied from its nighttime value of $\sim 0.6 \text{ km}^{-1}$ down to a minimum of $\sim 0.25 \text{ km}^{-1}$ at SZA $\sim 85^\circ$ near dusk or $\sim 75^\circ$ near dawn, rising again to (SZA-dependent) noon values of $\sim 0.35\text{--}0.5 \text{ km}^{-1}$. The results are interpreted through the geophysical effects controlling *D* region electrons, including the daytime dominant role of solar Lyman- α from low to mid-latitudes, and the greater role of GCR at increasingly higher mid-latitudes.

1. Introduction

Very Low Frequency (VLF) radio waves can propagate over very long distances (thousands of km) in the Earth-ionosphere waveguide bounded below by the Earth's surface (oceans/ground) and bounded above by the lowest edge of the Earth's ionosphere (the lower *D* region) at heights ~ 70 km by day and ~ 85 km by night. VLF radio propagation in the ionosphere is essentially controlled by free electrons; both positive and negative ions occur in comparable concentrations but have no significant effect at VLF because they are so much more massive than the free electrons (by factors of $>10,000$).

In the quiet *D* region there are two principal sources of free electrons. The main one at low and middle latitudes is UV from the daytime Sun, mainly Lyman- α , ionizing the minor neutral constituent NO (to $\text{NO}^+ + \text{e}^-$); this is generally important (and dominant) only above 65–70 km altitude because Lyman- α is absorbed by neutral O_2 below these heights (Banks & Kockarts, 1973). This absorption by O_2 also results in the ionization of NO being solar zenith angle (SZA) dependent and thus dependent on time of day and latitude.

The other important ionizing source is galactic cosmic rays (GCR) which ionize all the constituents in the neutral atmosphere, day and night, 24 hr a day. This ionizing process tends to be dominant below heights of 65–70 km at low to mid-latitudes because of the shielding effect of the Earth's geomagnetic field. In contrast, at mid-to high latitudes GCR ionization tends to dominate up to greater heights, 70–75 km or more, because of the lower shielding by the Earth's geomagnetic field there and the Sun being lower in the sky (i.e., higher SZA) resulting in more absorption of Lyman- α by O_2 . At night virtually all of the free electrons below ~ 75 km become effectively removed by rapidly attaching to the copious neutral O_2 molecules at these low altitudes forming negative ions. When daylight returns, visible light from the Sun releases these electrons again from the negative ions (Peterson, 1976; Reid, 1987; Thomas & Bowman, 1986; Thomas & Harrison, 1970; Verronen et al., 2006; see also Banks & Kockarts, 1973).

VLF propagation in the Earth-Ionosphere waveguide has been found to be normally remarkably stable in unperturbed conditions. Phase and amplitude perturbations in the propagation have thus been able to be used extensively to monitor external perturbations (in energy and height) such as from energetic particle (particularly electron) precipitation from the Earth's radiation belts into the top of the waveguide (e.g., Rodger et al., 2010). For convenience in making VLF propagation calculations, VLF observations have been used successfully to

characterize the electron densities in the lower D region by determining the “Wait” (Wait & Spies, 1964) height and sharpness parameters, H' and β , under a variety of daytime and nighttime conditions. These have included daytime at low latitudes (Thomson, 2010; Thomson et al., 2014), daytime at mid-latitudes (Thomson et al., 2011a, 2017), and nighttime (Thomson et al., 2007; Thomson & McRae, 2009), all of which used narrow-band VLF transmissions from man-made transmitters. Broadband VLF from lightning has been used to make similar measurements mainly over the US continental land mass (Cummer et al., 1998; Cheng et al., 2006 at night; Han & Cummer, 2010 by day).

VLF propagation techniques have recently been used to determine D region parameters by Kumar and Kumar (2020) and Chand and Kumar (2021) using VLF man-made transmitters received in the South Pacific. VLF techniques have also recently been used by McCormick & Cohen, 2021 testing a new four-parameter H'/β model for the D region, by Zhou et al. (2021) using timing of first and second lightning hops, and by Chowdhury et al. (2021) from the International Reference Ionosphere (IRI-2016, Bilitza, 2017) with VLF validation. Additionally, VLF techniques have been used by Rozhnoi et al. (2020), Barman et al. (2024), and Basak et al. (2024) to study solar eclipses, by Macotela et al. (2021) reporting a daytime spring-fall amplitude asymmetry, and by Xu et al. (2021) and Worthington and Cohen (2021) using VLF trans-ionospheric propagation together with the rocket-based Faraday International Reference Ionosphere electron density model (FIRI, e.g., Friedrich et al., 2018).

The determination and validation of energetic electron precipitation characteristics impacting the atmosphere has been identified as a key component of solar forcing descriptions in coupled-climate modeling studies (Funke et al., 2024; Matthes et al., 2017). The use of VLF propagation measurements to calculate electron precipitation fluxes has been an important factor in these efforts. Similarly effects of solar flares have been extensively monitored (e.g., Thomson & Clilverd, 2001; Thomson et al., 2005), as have occasional extra-galactic gamma-ray bursts (e.g., Fishman & Inan, 1988; Pal et al., 2023). Both the World-Wide Lightning Location Network (WWLLN, e.g., Rodger et al., 2005) and the Global Lightning Data set (GLD360, e.g., Said et al., 2010) rely on VLF radio waves radiated from lightning flashes propagating up to many thousands of km to the VLF receivers of their global networks. The world's great naval powers communicate with their submarines from some of the same large man-made VLF transmitters we use here. They make use of the large horizontal ranges (many thousands of km) and the ability of very low frequencies to penetrate seawater so allowing their submarines to remain submerged.

However, such efforts have been hampered by the difficulties in understanding propagation conditions near sunrise and sunset (Clilverd et al., 2010; Neal et al., 2015). A lack of detailed knowledge of VLF propagation conditions around sunrise and sunset has also restricted electron precipitation validation studies (Clilverd et al., 2020). For many years, distinctive VLF anomalies have been observed on (long) propagation paths that travel across a dawn/dusk terminator, particularly at dawn (Crombie, 1964). These involve clear successive minima in amplitude, known as modal minima, likely caused by destructive interference between new modes generated by the D region characteristics rapidly changing with distance as the waves travel across the terminator. These amplitude minima are often accompanied by rapid phase changes known as cycle slips. Recently Chand and Kumar (2017) reported and discussed similar observations on long VLF paths recorded at Fiji in the South Pacific. Quantitative explanations of these anomalies have been hindered by lack of D region propagation characteristics at dawn and dusk. In many of these cases the VLF waves will at times travel from a nighttime region of the Earth to a daytime region or vice-versa and so will propagate through a dawn/dusk transition requiring a model of the appropriate dawn/dusk ionosphere in this transition region for predicting phase and amplitude (as a function of time) at the receiver, to compare with observations.

However, very little attention has been given to characterize the D region in the dawn and dusk transition regions between day and night. Hence observations of the D region near dawn and dusk, as here, are very desirable for modeling and testing potential mechanisms in these transition regions.

A key aim of the current work is to provide the measurements to facilitate the modelling of dawn and dusk propagation conditions. Such measurements will extend the capabilities of VLF propagation monitoring for geophysical phenomena such as lightning, solar flares, solar eclipses, geomagnetic storms, substorms, and energetic particle precipitation. In order to accurately model propagation conditions over a wide range of SZA, observations from specific transmitter–receiver paths with near-constant SZA along the whole path are analysed. Interpretation is made using long-wave propagation codes. The selection and modelling of these paths are

described in Section 2. The delicate balance between solar UV and galactic cosmic ray effects is investigated within three different latitude bands. Section 3 presents the results for mid-latitude paths, with detailed analysis of specific paths. Section 4 present results for the low-latitude paths, while Section 5 presents results for the high latitude paths. The results are discussed in Section 6, including comparisons between dawn/dusk conditions relative to the overall diurnal variations, and existing rocket measurements. Summary and conclusions are given in Section 7.

2. Methods

2.1. Selecting Paths for VLF Observations

For a typical VLF path, at a fixed time of day, the SZA varies along the path from transmitter to receiver making it not straightforward to determine the characteristics at a particular SZA. Paths greater in length than $\sim 1,000$ km typically needed to be specifically chosen such that, at some convenient time of year when suitable VLF data was available, the SZA varied very little along the path at fixed times. This is particularly the case for dawn or dusk, so that the characteristics of the path at particular SZA could be determined. This meant that the path needed to align at least approximately with the sunrise or sunset, day/night-terminator at that time of year. The “convenient time of year” was preferably in the $< \sim 6$ months of the year closest to summer solstice for calibrating the path's VLF propagation using mid-day observations. The paths so chosen are shown in Figure 1. These include two very short paths (~ 300 km), from NPM in Hawaii (Thomson et al., 2014) and from NWC, North West Cape, Australia (Thomson et al., 2012, 2014). For these the SZA varies very little along their short paths (which also happen to be at low latitudes). The receivers at Eskdalemuir, St. John's, Reykjavik and Dunedin are part of the AARDDVARK network (Antarctic-Arctic Radiation-belt (Dynamic) Deposition-VLF Atmospheric Research Consortium: for example, Clilverd et al., 2009; http://www.physics.otago.ac.nz/space/AARDDVARK_homepage.htm).

2.2. Determining D Region Parameters, H' and β , From the VLF Observations

US Navy modal waveguide codes, ModeFinder (Morfitt & Shellman, 1976) and LWPC (Long Wavelength Propagation Capability, Ferguson & Snyder, 1990; see also Ferguson, 1998) are both designed to calculate phase (degrees) and amplitude ($\text{dB} > 1 \mu\text{V/m}$) as functions of distance when supplied with transmitter frequency, radiated power and ionospheric D region characteristics, H' and β , or (particularly for ModeFinder) an electron density versus height profile. The observed phase and amplitude, on each path at each time, are then compared with calculated values over appropriate ranges of H' and β , to determine the actual H' and β at that time on that path, as detailed in Sections 3, 4, and 5 below. The H' and β so determined for each path at each time are thus their averages along the path for each (constant) SZA. There will, in reality, be some variation along these paths due to the latitudinal dependence of GCR as mentioned in the Introduction above and in Section 6.1 below.

Quite often there is not much to choose between ModeFinder and LWPC; they both give very similar results under most conditions (e.g., Thomson et al., 2017). Some considerations in choosing, taken into account here, are briefly discussed below in Section 6.3.

3. Results: Mid-Latitude Observations

3.1. NSY, on Sicily in the Mediterranean, to Cambridge, UK

Figure 2 shows the morning (0–12 UT) phase and amplitude observations (top panels) recorded at Oakington (52.26°N , 0.07°E), near ($< \sim 10$ km N.W. of) Cambridge, UK, in the summer of 2005 (30 July to 4 August) transmitted from the 45.9 kHz transmitter, NSY (37.13°N , 14.44°E), 2023 km to the southeast as shown in Figure 1a. VLF phase plots, such as those here, typically need to be corrected (adjusted), for convenience, for small, fairly constant phase drifts and occasional (often random) phase jumps, normally at the transmitter, to allow the resulting daily phase plots, over several days, to superpose (approximately) as in Figure 2. Here, for NSY-Oakington, no phase drift correction was actually needed, and the only phase jumps needing correction were a very small number involving only multiples of 180° which is common for MSK modulation (e.g., Thomson, 2010) as used by all the VLF transmitters here. The middle panels of Figure 2 show the same phase and amplitude observations but with an expanded time scale about dawn (~ 3.2 – 4.6 UT) with SZA = 90° , 97° , and 98° being indicated with vertical dashed lines. The path was fairly well aligned with the sunrise terminator (see Figure S1a in Supporting Information S1, together with Figures S1b, S1c, S1d ... S1k in Supporting Information S1 for

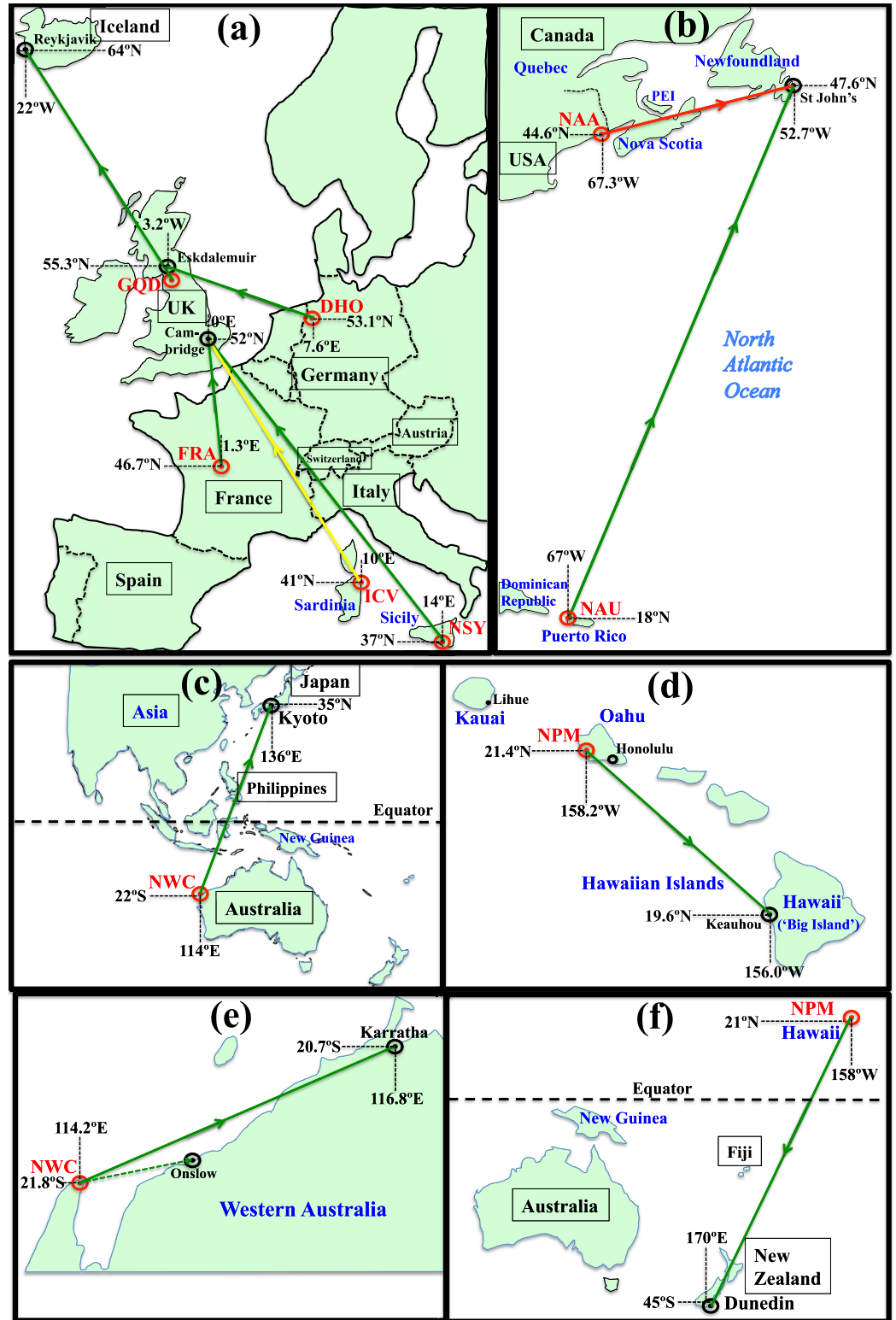


Figure 1. Very low frequency paths used here to determine ionospheric D region characteristics particularly around dawn and dusk.

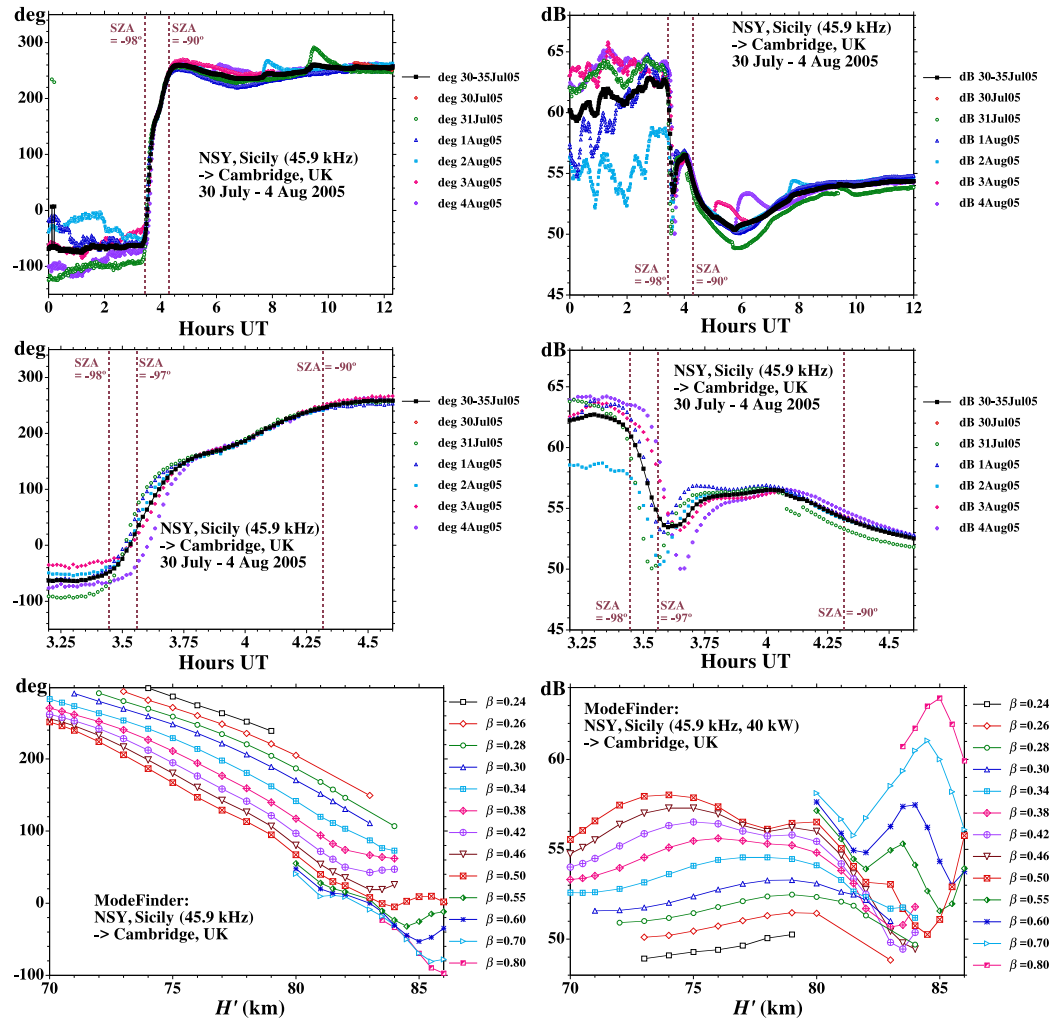


Figure 2. (Top two panels) Phase (degrees) and amplitude (dB) observed at Oakington, Cambridge, UK, versus time (0–12 UT) received from the 45.9 kHz transmitter NSY near Niscemi, Sicily, 30 July–4 August 2005. (Middle two panels) Same data as in the top two panels but for an expanded time scale about dawn (3.2–4.6 UT). (Bottom two panels) ModeFinder calculations for this path of the phase (degrees) and amplitude (dB > 1 $\mu\text{V}/\text{m}$) as functions of height, H' and sharpness, β .

all 11 paths); at dawn the SZA varied by $\sim 2.5^\circ$ ($-90^\circ \pm 1.2^\circ$) along the 2023-km path, while near SZA $\approx 97.5^\circ$, it varied by only $\sim 0.4^\circ$ along the path. Also shown in Figure 2 (bottom panels) are ModeFinder calculations of the phases and amplitudes of NSY to be expected near Cambridge for a range of appropriate parameters H' and β for the D region. The observational plots in the upper panels have been calibrated (by vertically shifting each whole plot) so that their mid-day values match the calculated values in the lower panels for $H' = 70.8$ km and $\beta = 0.42$ km $^{-1}$; these H' and β values were estimated for the NSY–Cambridge path here from the calibrated VLF observations of Thomson et al. (2011a, 2012). This removes the need to know the actual power and phase radiated at the NSY transmitter.

The observed phase in degrees together with the observed amplitude in dB at particular UT times in the upper panels were then used in the bottom panels to find the values of H' and β at each of these selected UT times. The SZA at the mid-point of the NSY–Oakington path was then determined at that time from either NOAA’s SZA calculator (<https://gml.noaa.gov/grad/solcalc>) or, in particular from their spreadsheets (<https://gml.noaa.gov/grad/solcalc/calcdetails.html>), or from “Google Earth” by measuring the distance in degrees from the path mid-point to the sub-solar point on the Earth’s surface for the relevant time and date. The resulting values of H' and β as functions of SZA are shown plotted in the top, left-hand panels of Figure 3 (for H') and Figure 4 (for β) with black lines and black square plot symbols. The SZA values in degrees are shown as negative before mid-day and

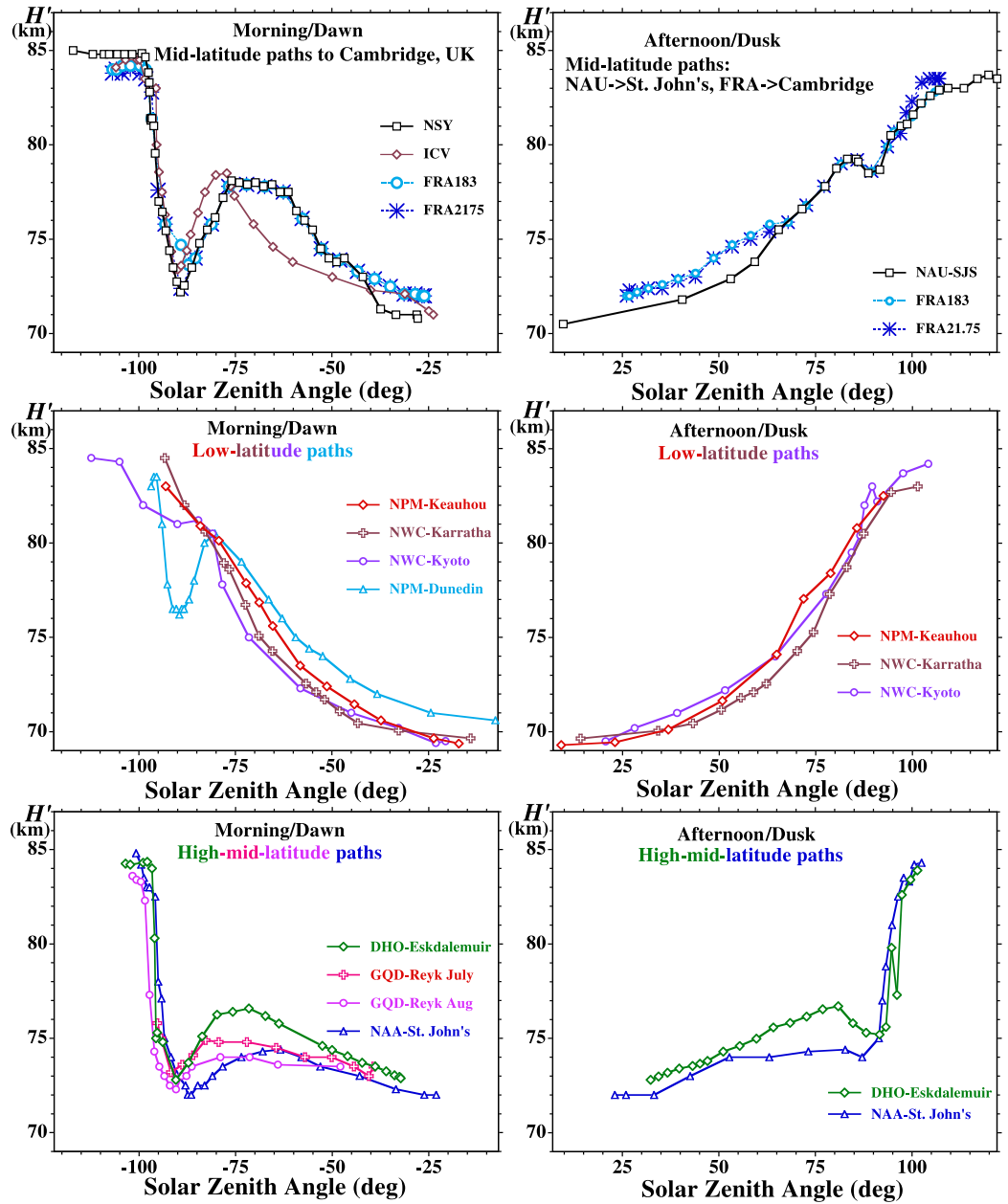


Figure 3. Height parameter, H' versus solar zenith angle (SZA) inferred from very low frequency observations (Top two panels) Mid-latitude values of H' versus SZA for morning/dawn (left) and afternoon/dusk (right). (Middle two panels) Low latitude values of H' versus SZA for morning/dawn (left) and afternoon/dusk (right). (Bottom two panels) High mid-latitude values of H' versus SZA for morning/dawn (left) and afternoon/dusk (right).

positive after mid-day in this report. Note that at night, on the far left of these plots, $H' = \sim 85$ km and $\beta = \sim 0.7$ km⁻¹, very similar to previous observations (Thomson et al., 2007; Thomson & McRae, 2009), while at mid-day, $H' = \sim 70.8$ km and $\beta = \sim 0.42$ km⁻¹ as discussed above. Note, in particular, the clear minimum at $H' = \sim 72.5$ km near dawn (SZA $\approx -90^\circ$).

As can be seen in the middle panels of Figure 2, both the amplitude and phase of NSY recorded at Cambridge start responding to the approach of dawn when the SZA at the mid-point is between -98.0° and -97.5° . As mentioned above the variation of SZA along the path is only $\sim 0.4^\circ$ in these conditions. In comparison, Reid (1987) reported the average pre-dawn onset of mesospheric echoes from the 50-MHz radar at Poker Flat in Alaska occurred around a mean SZA of 94° with only 7% of echoes occurring with SZA $> 96^\circ$. Reid (1987) also cites

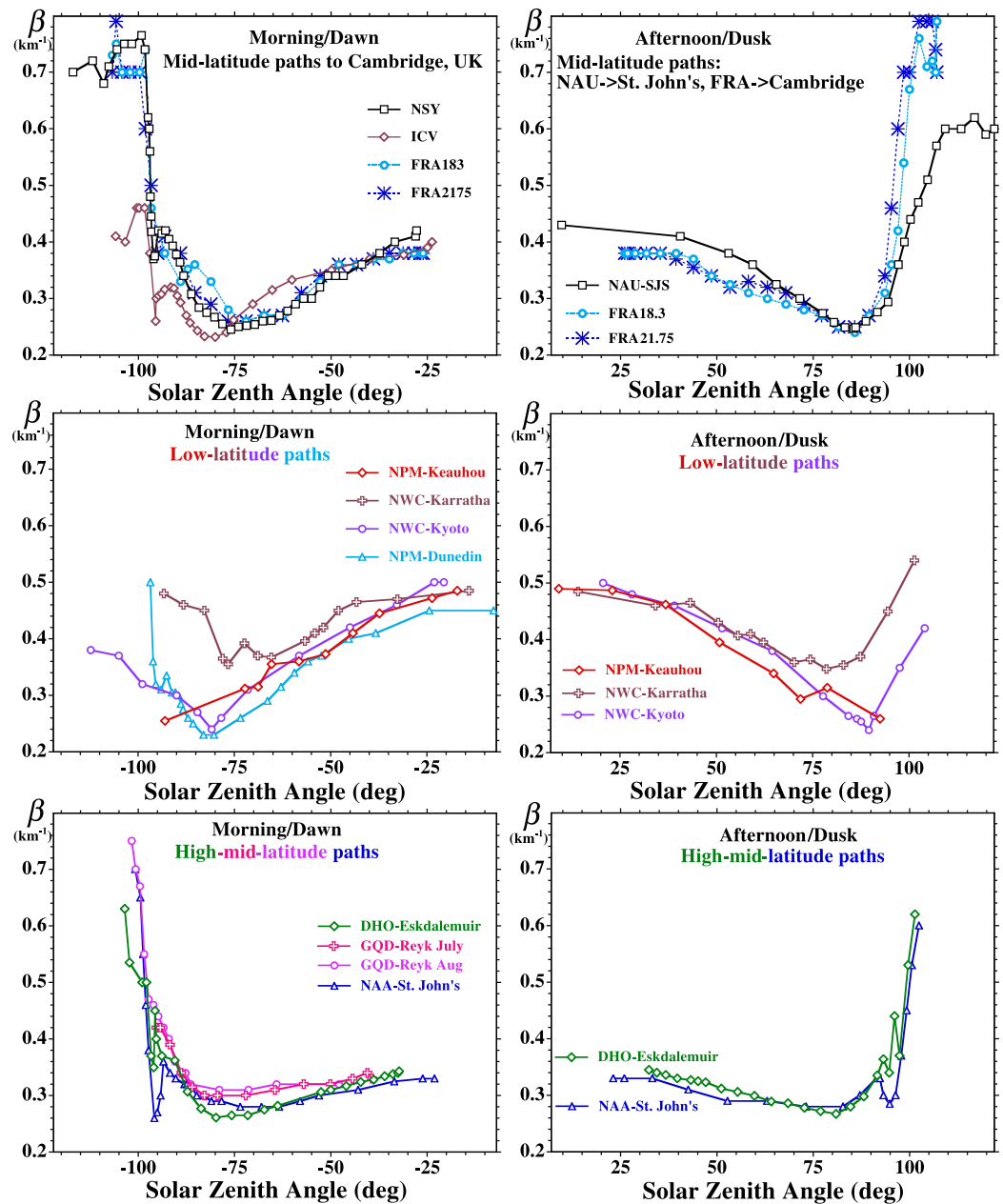


Figure 4. Sharpness parameter, β , versus solar zenith angle (SZA) inferred from very low frequency observations (Top two panels) Mid-latitude values of β versus SZA for morning/dawn (left) and afternoon/dusk (right). (Middle two panels) Low latitude values of β versus SZA for morning/dawn (left) and afternoon/dusk (right). (Bottom two panels) High mid-latitude values of β versus SZA for morning/dawn (left) and afternoon/dusk (right).

Sechrist (1968) as reporting VLF observations (amplitude only) at Wallops Island, Virginia, showing pre-dawn changes at 94° , and on one occasion at 98° . However, as discussed further below in Section 6.5, Thomas and Harrison (1970) found, using VLF and LF measurements on paths in the UK, that the pre-dawn changes in the D region started at $SZA \sim 98^\circ$, very similar to the NSY-Cambridge result found here.

3.2. ICV, On Sardinia in the Mediterranean, to Cambridge, UK

Figure S2 in Supporting Information S1, in the Supporting Information, shows the phase and amplitude observations (top and middle panels) recorded at Oakington near Cambridge, UK, in the summer of 2005 (26 June–1 July) transmitted from the 20.27-kHz transmitter, ICV (40.92°N , 9.73°E), 1,459 km approximately to the

southeast as shown in Figure 1a. Also shown in Figure S2 in Supporting Information S1 (bottom panels) are ModeFinder calculations of the phases and amplitudes of ICV to be expected at Oakington for a range of appropriate H' and β for these conditions. The observations in the upper panels have been calibrated by vertically shifting so that their mid-day values match the calculated values in the bottom panels for $H' = 71.0$ km and $\beta = 0.40$ km⁻¹. These H' and β values were estimated for the ICV-Cambridge path here from the calibrated VLF observations of Thomson et al. (2011a, 2012). As for most of the other transmitter-receiver-pair recordings used here (including NSY, Sicily, in Section 3.1 above), this removes the need to know the actual power and phase radiated at the transmitter.

As with NSY-Oakington above, H' and β as functions of SZA were determined and are plotted in the same (top, left-hand) panels of Figures 3 and 4 used in Section 3.1 but with brown lines and brown diamond plot symbols. Clearly both the NSY and ICV plots are rather similar though the ICV minimum in H' near dawn is slightly less deep (~ 73.5 km as opposed to ~ 72.5 km). Although both paths pass over the southern European (Swiss-French-Italian) Alps, the NSY path is longer but has an alpine section which is much shorter than the ICV path's alpine section (which runs along the mountainous French-Italian) border. The NSY path results will thus be assumed to be likely to be more reliable than the ICV results.

3.3. Central France Northwards to Cambridge, UK (~600 km)

The VLF transmitter at 46.71°N, 1.25°E (in central France near Rosnay), is referred here to as “FRA”, as it was in Thomson (1993). Two recorded periods are used here: for the first, 14–20 June 2005, FRA was radiating on 21.75 kHz while for the second, 20–26 June 2005, FRA radiated on 18.3 kHz. The path is shown in Figure 1a. Unfortunately FRA was not using a conventional stable phase, but rather its phase was continually (quasi-) randomly scattered. Our receivers could track this and so we could record valid amplitudes but the phase itself was too unpredictable for us to use. This phase issue might have been resolvable but, at the time, we were unable to record the phase close to the transmitter as well as at the receiver at Oakington. Hence we use only amplitude for FRA-Oakington here; thus the observational plots and ModeFinder calculation plots in Figure S3 in Supporting Information S1 are for amplitude only. To enable β to be determined, H' was assumed to vary with SZA as for NSY-Oakington except that in some instances H' needed to be adjusted slightly, for example, at mid-day where $H' = 72.0$ km and $\beta = 0.38$ km⁻¹ was estimated from Thomson et al. (2011a, 2012). The resulting H' and β as functions of SZA are plotted in the same (top, left-hand) panels of Figures 3 and 4 used in Section 3.1 but using cyan (18.3 kHz) and blue (21.75 kHz) for the lines and plot symbols. While the H' plots for the two FRA frequencies are necessarily rather similar to the corresponding NSY plot (because both are derived from the NSY H' data), the β plots are rather similar too indicating the FRA data is providing some support through its apparent consistency with the NSY and ICV data.

3.4. NAU, Puerto Rico, Caribbean, to St. John's, NFL, Canada (~3,500 km)

Figure S4 in Supporting Information S1 shows phase and amplitude observations (upper panels) recorded at St John's (47.60°N, 52.68°W), Newfoundland, Canada, 11–18 June 2013, from the 40.75 kHz transmitter, NAU (18.40°N, 67.18°W), 3,497 km to the southwest as shown in Figure 1b. The data are analysed during the period around dusk in June, when the SZA varied by only $\sim 4^\circ$ ($\sim 90^\circ \pm 2.5^\circ$) along the 3,497-km path. Also shown in Figure S4 in Supporting Information S1 (bottom panels) are the appropriate ModeFinder calculations of the phases and amplitudes. Again, the observational plots in the upper panels have been calibrated (by vertically shifting each whole plot) so that their mid-day values match the calculated values in the bottom panels for $H' = 70.5$ km and $\beta = 0.43$ km⁻¹, as in Thomson et al. (2014).

The resulting values of H' and β as functions of SZA, which have previously been reported in Thomson et al. (2014), are shown plotted in a slightly different form and to higher values of SZA, in the top, right-hand panels of Figure 3 (for H') and Figure 4 (for β) with the black line and black square plot symbols. Note that at night, on the far right of these plots, $H' = \sim 84$ km and $\beta = \sim 0.6$ km⁻¹, in line with previous observations on other paths (Thomson et al., 2007; Thomson & McRae, 2009), while at mid-day, $H' = \sim 70.5$ km and $\beta = \sim 0.43$ km⁻¹ as discussed above. Note, in particular, there is no deep minimum near dusk (SZA = 90°), like that of $H' = \sim 73$ km near dawn in the top-left panel of Figure 3. The dusk variation of H' versus SZA shown here is, in fact, quite similar to that reported by Thomson (1993) from other earlier paths.

3.5. Central France Northwards to Cambridge, UK (~600 km)

As in Section 3.3 above, we again use only amplitude for FRA-Oakington, using the plots in the top panels of Figure S3 in Supporting Information S1 but for dusk rather than dawn. To enable β to be determined, H' at dusk was assumed to vary with SZA as for NAU to St. John's (as in Section 3.4 above) except that again, in some instances, H' needed to be adjusted slightly, for example, at mid-day where again we took $H' = 72.0$ km and $\beta = 0.38$ km⁻¹ for FRA-Oakington. The resulting H' and β as functions of SZA are plotted in the same (top, right-hand) panels of Figures 3 and 4 used in Section 3.4 but using cyan (18.3 kHz) and blue (21.75 kHz) for the lines and plot symbols. While the H' plots for the two FRA frequencies are necessarily rather similar to the corresponding NAU plot (because both are derived from the NAU H' -data), the β plots can be seen to be rather similar too, indicating the FRA data is again providing some support by being consistent with the NAU data.

4. Results: Low Latitude Observations

4.1. NPM, Oahu, Hawaii, to Keauhou, Big Island, Hawaii (306 km)

Thomson et al. (2014, Figure 4) measured the phase and amplitude of the 21.4 kHz U.S. Navy transmitter, NPM (21.42°N, 158.15°W) on Oahu, as received, 306 km away over a nearly all-sea path, at Keauhou (19.58°N, 155.97°W) on the west coast of the “Big Island” of Hawaii (Figure 1d), in the period 19–25 August 2012. These measurements were then used, together with ModeFinder calculations, to determine H' and β as functions of SZA at this low latitude, ~20°N (geographic and geomagnetic: <https://www.ncei.noaa.gov/sites/default/files/2022-03/GeomagneticCoordinates.pdf>). These H' and β values are plotted as red lines with red diamond plot symbols in the middle panels of Figures 3 and 4 respectively, on the left for the morning values and on the right for the afternoon values. Two extra dB/deg data points, one from 16 UT (87 dB, 40°) and the other from 5 UT \equiv 29 UT (86 dB, 54°) from Thomson et al. (2014; Figure 4) were used here with the extended, NPM-Keauhou, ModeFinder plots in Figure S5 in Supporting Information S1 to generate the two extra SZA data points ($H' = 83.0$ km, $\beta = 0.255$ km⁻¹ and $H' = 82.5$ km, $\beta = 0.260$ km⁻¹) not shown in Thomson et al. (2014) but shown in Figures 3 and 4 here. It is immediately clear in Figure 3 that, for H' , the clear minimum (~73 km) at dawn at mid-latitudes does not occur for the low latitude of Hawaii while, in the afternoon and at dusk (top and middle, right-hand panels), the variation of H' with SZA shows similarities at both mid- and low latitudes.

4.2. NWC, North West Cape, Australia, to Karratha, Australia (300 km)

As well as reporting VLF measurements of NPM in Hawaii together with the resulting H' and β as functions of SZA used in Section 4.1 above, Thomson et al. (2014) also compared these with H' and β as functions of SZA for the ~300-km, low latitude path from NWC (21.82°S, 114.17°E) to Karratha (Millars Well, 20.74°S, 116.82°E) in northwest Australia (Figure 1e) in October 2011. Figure S6 in Supporting Information S1 (top panels) shows the underlying phase and amplitude measurements together with (lower panels) the appropriate ModeFinder calculations used there and further used again here to extend the H' and β results to slightly higher SZA's (similar to the small extensions for NPM in Section 4.1 above). More details about these NWC-Karratha observational techniques are given by Thomson et al. (2012); the techniques were very similar to those for NPM-Keauhou, above.

These H' and β values are plotted as functions of SZA using brown lines with open “+” plot symbols in the middle panels of Figures 3 and 4 respectively, on the left for the morning values and on the right for the afternoon values. It can thus be seen that the H' plots for NWC-Karratha are rather similar to those for NPM-Keauhou; in particular neither of these two low latitude plots shows the marked minimum at dawn which was apparent for the mid-latitude paths (NSY and ICV to Oakington). The geographic latitude of the NWC-Karratha path (~20°S) is very similar in magnitude to the geographic latitude of the NPM-Keauhou path (~20°N) but the magnitude of the geomagnetic latitude of the NWC path is quite a bit higher, ~31°S (vs. 20° for the NPM path). Thus the increased GCR at this somewhat higher latitude is not sufficient to produce a discernable dawn minimum.

4.3. NWC, North West Cape, Australia, to Uji, Kyoto, Japan (6,680 km)

Araki et al. (1969) reported the variations with time (JST = UT + 9) of the observed average phase and amplitude of NWC, when radiating on 15.5 kHz, across the equator (Araki, 1973), and observed at Uji (34°54'N, 135°48'E), Kyoto, Japan (Figure 1c), during the period 31 July–7 August 1968. The path was fairly closely aligned with the

dusk terminator during this period; the alignment with the dawn terminator was only rather approximate but the absence of clear mode conversion effects near dawn probably indicates that the alignment will none-the-less suffice.

The bottom two panels of Figure S7 in Supporting Information S1 show the results of LWPC calculations of phase, in degrees, and amplitude, in dB $> 1 \mu\text{V/m}$, for appropriate values of H' and β for a radiated power of 1.0 MW at 15.5 kHz. From Thomson et al. (2012), the (average) mid-day parameters for the D region on this trans-equatorial path in 1968 (high solar maximum) were estimated to be $H' = 69.5 \text{ km}$ and $\beta = 0.50 \text{ km}^{-1}$, which, as can be seen in the LWPC-calculated plots in the (bottom panels) of Figure S7 in Supporting Information S1, gives 29° and 66.5 dB at mid-day. These two values were then used to normalize the phase and amplitude observations in Araki et al. (1969) which are shown, as functions of JST, in the top two panels of Figure S7 in Supporting Information S1, thus enabling H' and β to be determined, from the bottom panels, for each time (and hence subsequently each SZA), in a similar way to that in Section 3.1. The resulting H' and β as functions of SZA (many of which were reported in Thomson et al., 2014) are shown, using violet lines with violet circles as plot symbols in the middle two panels of Figures 3 and 4 respectively, on the left for the morning values and on the right for the afternoon values. Again there is no minimum in H' near dawn for this fairly low latitude trans-equatorial path as was also seen for the other low latitude paths above (Sections 4.1 and 4.2). The geomagnetic latitude of Kyoto is also low at about 26°N .

4.4. NPM, Oahu, Hawaii, to Dunedin, NZ (8,090 km)

The path from NPM in Hawaii to Dunedin, NZ (Thomson et al., 2011b, 2012) is mainly low latitude (Figure 1f), passing \sim southwest across the equator, but becomes mid-latitude for the final part from $\sim 30^\circ\text{S}$ to the Dunedin receiver (45.79°S , 170.48°E), for which the geomagnetic latitude is $\sim 49^\circ\text{S}$ (<https://www.ncei.noaa.gov/sites/default/files/2022-03/GeomagneticCoordinates.pdf>).

Figure S8 in Supporting Information S1 (upper four panels) shows the measured phases and amplitudes (normalized at mid-day to 378° and 53.2 dB (using $H' = 70.6 \text{ km}$ and $\beta = 0.45 \text{ km}^{-1}$), as functions of time-of-day, in UT, for the period 16–22 January 2017 UT during which the dawn terminator is fairly closely aligned with this ($\sim 8.1 \text{ Mm}$) path. Also shown (two bottom panels) are LWPC calculations for phase and amplitude at Dunedin for a range of appropriate values (as averages along the path) of H' and β , thus enabling specific values of H' and β , to be determined for a range of morning values of UT and hence SZA. These are shown plotted in the middle, left-hand panels of Figures 3 and 4, respectively, from which it can be seen that there is a minimum at dawn ($\text{SZA} = -90^\circ$, $H' = \sim 76.5 \text{ km}$), but this minimum is markedly less deep than that ($H' = \sim 73 \text{ km}$) for a fully mid-latitude path (e.g., NSY-Oakington, top left panel Figure 3), consistent with the NPM-Dunedin path being partly at mid-latitudes, though mainly at low latitudes where GCR electrons are contributing only modestly to the lowest ionosphere.

5. Results: High Mid-Latitude Observations ($\sim 53^\circ$ – 65° Geomagnetic)

5.1. DHO, North Germany to Eskdalemuir, Scotland (748 km)

As shown in Figure 1a, VLF transmissions from DHO (53.08°N , 7.61°E) after travelling 748 km, mainly across the North Sea, were recorded at Eskdalemuir (55.31°N , 3.21°W) in Scotland, during the period 4–19 July 2015 UT. These recordings were used in Thomson et al. (2017) to determine H' and β , for this high mid-latitude path, as functions of SZA up to $\sim 75^\circ$. Here these results are extended to SZA's beyond 90° . Figure S9 in Supporting Information S1 (upper four panels) shows the measured phases and amplitudes as functions of UT, normalized at mid-day as in Thomson et al. (2017), at 120° and 68.8 dB using $H' = 72.8 \text{ km}$ and $\beta = 0.345 \text{ km}^{-1}$ in ModeFinder; also shown (bottom two panels) are plots of ModeFinder-calculated phases and amplitudes for appropriate ranges of H' and β .

The bottom left-hand panels of Figures 3 and 4 show, as green lines and diamond plot symbols, the resulting morning values of H' and β as functions of SZA for the DHO-Eskdalemuir path. As can be seen, this high mid-latitude path also shows a deep minimum in H' at dawn ($\text{SZA} = -90^\circ$, $H' = \sim 72.8 \text{ km}$), consistent with enhanced electron density in the lowest D region, as the visible light of dawn releases electrons, generated overnight by GCR, from their attached negative ions. The bottom right-hand panels of Figures 3 and 4 show the resulting afternoon values of H' and β as functions of SZA for the DHO-Eskdalemuir path. The dawn terminator is fairly

well aligned with the path during the July measurements here; the SZA varies by only $\sim 3.5^\circ$ along the path at dawn (SZA $\sim -90^\circ$). At dusk it is not well aligned with the dusk terminator, but the path is short resulting in the SZA at dusk varying only $\sim 6.5^\circ$ along its 748-km length. It thus seems likely that mode conversion should not be too significant, at least below SZA $\sim +90^\circ$, before β starts to change more rapidly with SZA.

5.2. NAA, Maine, USA, to St. John's, Newfoundland, Canada (1,173 km)

As indicated in Figure 1b, VLF transmissions from NAA (44.64°N, 67.28°W), after travelling over a mixed land-sea path, were recorded at St. John's, Newfoundland (47.60°N, 52.68°W) during the period 1–28 June 2019. The SZA changes along the length of this 1173-km path by $\sim 10^\circ$ near dawn and by $\sim 7^\circ$ near dusk. The path is $\sim 50\%$ over the sea and $\sim 50\%$ over land; this land has low electrical conductivity (ITU-R, 2015; Morgan, 1968) mainly ~ 0.001 S/m but some parts have ~ 0.0003 S/m near St. John's (compared with western Europe at mainly ~ 0.01 S/m). Figure S10 in Supporting Information S1 (upper four panels) shows the measured phases and amplitudes as functions of UT, normalized at mid-day as in Thomson et al. (2017), at 313° and 74.8 dB using $H' = 72.0$ km and $\beta = 0.33$ km $^{-1}$ in LWPC; also shown (lower two panels) are plots of LWPC-calculated phases and amplitudes for appropriate ranges of H' and β . The resulting morning values of H' and β as functions of SZA for the NAA-St. John's path are shown in blue (triangular plot symbols) in the left-hand bottom panels of Figures 3 and 4 respectively while the corresponding plots for the afternoon values are shown in the right-hand bottom panels. Interestingly there are small, marginally significant, minima at dusk (SZA = $+90^\circ$) in both of the H' curves at high-mid-latitude (NAA-St. John's and DHO-Eskdalemuir); these small minima may not be significant or may be due to mode-conversion discussed briefly in Section 6.1 below.

5.3. 22.1 kHz From Skelton, North England, to Reykjavik, Iceland (1,487 km)

The 22.1-kHz transmitter at 54.73°N, 2.88°W near Skelton, Cumbria, England, is referred to here as “GQD” as in Thomson et al. (2018) and in Koh et al. (2019). This same 22.1-kHz transmitter near Skelton has also been referred to as “GVT” (e.g., Clilverd et al., 2020). The 1478-km path from GQD, Skelton, to Reykjavik (64.11°N, 21.79°W) travels \sim northwest over Scotland (Figure 1a) but is $\sim 75\%$ over the sea, with $< 10\%$ of the path over low conductivity ground (~ 0.001 S/m), and with the rest of the land with good conductivity (0.01 S/m). Results from this path have been reported by Thomson et al. (2018) but a wider range of times-of-day and SZA are used here. Figure S11 in Supporting Information S1 shows (upper four panels) the measured phases and amplitudes as functions of UT, for the periods 19–25 July 2016 and 19–25 August 2016 normalized at mid-day for the July period at 11.5° and 64.6 dB using $H' = 73.5$ km and $\beta = 0.33$ km $^{-1}$ in LWPC and for the August period at 14.5° and 64.5 dB using $H' = 73.5$ km and $\beta = 0.32$ km $^{-1}$ in LWPC; also shown (lowest two panels) are plots of LWPC-calculated phases and amplitudes for appropriate ranges of H' and β . The resulting morning values of H' and β , as functions of SZA for this GQD-Reykjavik path, are shown in the bottom left-hand panels of Figures 3 and 4 respectively. The dawn terminator is well aligned with the path during the July period but somewhat less so for August; the SZA varies by only $\sim 1^\circ$ along the path at dawn (SZA $\sim -90^\circ$) in July but for August varies $\sim 5^\circ$.

6. Discussion

Dawn/dusk propagation conditions have been considered for three separate latitudinal ranges. The assumption made is that latitudinal differences in the D-region response to solar EUV and GCR forcing are large in comparison to any longitudinal variations. However, we note here that the low-latitude analysis presented here uses paths that are primarily focused on the Pacific region, while the mid and mid-high latitude analysis relies on paths focused on the North Atlantic region. This experimental restriction on any longitudinal interpretation is an area for future work, requiring new data sets to be developed. At mid-high latitudes the balance between geographic coordinate systems and geomagnetic coordinate systems could be a factor in considering longitudinal variations in D-region responses to dawn/dusk conditions, especially in response to the geomagnetic field effect on GCR intensity. An example of this is shown in Figure 3 of Clilverd et al. (1991) where geomagnetic longitude contours (in the form of L-shell contours) are over-plotted on a geographic map and show substantial variations in the Atlantic region compared with the Pacific. Never-the-less, the analysis presented here clearly shows the importance of SZA on D-region electron concentration profiles, as is discussed in more detail below.

6.1. Dependency of H' on SZA

In Figure 3, aside from the pronounced minima at dawn ($SZA = -90^\circ$) at mid-latitudes, the variations of H' with SZA are observed to be broadly quasi-Chapman-like as reported by Thomson (1993). Away from dawn and dusk, D region electron density profiles, at least at low and middle latitudes, are largely generated by 121.6 nm solar Lyman- α ionizing the minor neutral constituent $NO \rightarrow NO^+ + e^-$, but with the Lyman- α depth penetration being controlled through absorption by the major neutral constituent O_2 (Banks & Kockarts, 1973). This results in Lyman- α ionization penetrating down to as low as ~ 70 km altitude at mid-day but to increasingly greater heights as the SZA increases towards dawn and dusk.

Below 65–70 km, ionization is dominated by GCR continuously (partially) ionizing all neutral constituents. This is essentially offset by the free electrons so generated rapidly becoming attached to some of the abundant neutral O_2 molecules forming negative ions, $O_2 + e^- + M \rightarrow O_2^- + M$, where M is another neutral molecule, typically O_2 or N_2 , enabling conservation of both momentum and energy (Banks & Kockarts, 1973). During the night these, in turn, exchange with other neutral species forming other (hydrated) negative ions such as CO_3^- and NO_3^- (e.g., Reid, 1976, 1987; Verronen et al., 2006) which, all being so much more massive than free electrons, have essentially no effect on VLF radio waves. Thus essentially no free electrons are observed at these low altitudes at night.

Photo-detachment at dawn from the CO_3^- -based ions requires only visible light while UV is needed for the NO_3^- -based ions. As dawn approaches, the first changes in the VLF phases and amplitudes are seen when the SZA is between -98° and -97.5° (Section 3.1 above) which is presumably due to visible light, because of the nearly horizontal incoming sunlight being depleted of UV by low altitude ozone (e.g., Macotela et al., 2019). Photo-detachment at dawn from the NO_3^- -based ions will presumably come later. Hence when sunlight returns around dawn, the electrons are photo-detached from these negative ions accumulated during the night, resulting in more cosmic ray generated free electrons at these low altitudes than at any other time of day and is likely to account for the marked minimum in H' of ~ 73 km seen at dawn at mid-latitudes in Figure 3. This is also believed to be the cause of the VLF phase overshoots often observed at dawn (e.g., Macotela et al., 2019, and references therein; see also, e.g., top left panels of Figure 2, Figure S2, S8, and S9 in Supporting Information S1). Detailed D -region chemistry simulations are required to definitively show that this is the cause. In contrast, no minimum in H' at dawn can be seen at low latitudes (middle, left-hand panel of Figure 3) for the observations of NPM in Hawaii or for the trans-equatorial path NWC to Kyoto ($\sim 31^\circ S$ through 0° to $26^\circ N$ geomagnetic), and only a tentative small minimum (at $H' \sim 81$ km) can be seen for the short NWC-Karratha path ($\sim 30^\circ S$). This is likely to be due to the markedly smaller galactic cosmic ray intensity at these low latitudes (Heaps, 1978; Neher & Anderson, 1962). This middle, left-hand panel of Figure 3 also shows a moderate dawn minimum (~ 76.5 km) for the trans-equatorial path NPM to Dunedin, NZ ($\sim 21^\circ N$ through 0° to $49^\circ S$ geomagnetic) for which $\sim 70\%$ is low latitude and $\sim 30\%$ is mid-latitude. Further, all the high mid-latitude paths in Figure 3 (bottom, left-hand panel) show the marked dawn minimum (72–73 km). In contrast, at dusk, in Figure 3 (right-hand panels) there are no minima in H' or only relatively minor (even tentative as in the top panel) minima (near $SZA = 90^\circ$). These latter minor minima may not be significant or may possibly be due to mode-conversion issues caused by rapidly changing H' and β near and after dusk. VLF mode-conversion (e.g., Pappert & Snyder, 1972) occurs when some property (e.g., H' , β , ground conductivity etc.) of the Earth-ionosphere waveguide changes over a short distance $< \sim \lambda$ (a wavelength) causing some power to scatter into one or more new modes resulting in interference between modes.

Figure 3 (bottom panels) also shows that, away from dawn and dusk, variations of H' with daytime SZA tend to be smaller at higher path latitudes probably mainly due to the greater influence of (SZA-independent) galactic cosmic ray electrons at these higher geomagnetic latitudes. At night, shortly before dawn, the H' values reported here are mainly 84–85 km consistent with the nighttime H' observations of Thomson et al. (2007) and Thomson & McRae (2009). Shortly after dusk they tend to be a little (~ 1 km) lower probably consistent with the D region taking up to ~ 1 –2 hr or so to settle into night conditions.

6.2. Dependency of β on SZA

Apart from near dawn and dusk, β shows the clear trend, in Figure 4, of decreasing with increasing SZA from a maximum near noon. This is due to the higher altitude Lyman- α electrons decreasing as the Sun gets lower in the sky while the lower altitude galactic cosmic ray electrons remain constant, being largely SZA independent (Thomson & Clilverd, 2001; Thomson et al., 2014). At dawn and dusk, as can be seen, β changes generally fairly

rapidly with SZA, particularly at dawn, from nighttime values of typically $\sim 0.6\text{--}0.8\text{ km}^{-1}$ to high-SZA daytime values of $\sim 0.25\text{--}0.3\text{ km}^{-1}$. Not all paths show nighttime β values of $\sim 0.6\text{--}0.8\text{ km}^{-1}$. There are a variety of reasons for this (which may also apply for nighttime values of H' here on these paths). In the case of the short path NPM-Keauhou, no automated recording was available and it was not convenient to continue the manual recordings at night. For the short path NWC-Karratha the situation was somewhat similar compounded, as discussed in Thomson et al. (2014), by low sky-wave amplitude and low ground conductivity. Trans-equatorial paths, such as NWC-Kyoto and NPM-Dunedin used here, have been found to be frequently anomalous at night though not by day nor, as found here, largely not during dawn/dusk transitions. As noted above, the path ICV-Cambridge (Section 3.2) with significant parts over mountain ranges and the path NAA-St. John's (Section 5.2) largely over low conductivity ground are also liable to have nighttime anomalies (Thomson et al., 2007; Thomson & McRae, 2009). None-the-less, the paths NSY and FRA to Cambridge, NAU to St. John's, DHO to Eskdalemuir and GQD to Reykjavik (in August) here provided regular nighttime parameters (even though the night was fairly short for the last two).

6.3. Early US Navy Recommendations and Waveguide Codes

The US Navy's LWPC propagation code for VLF contains an optional "LWPM" ionospheric model which has some limited SZA-dependence (Ferguson, 1998). In this model, H' and β are constants by day at 74 km and 0.3 km^{-1} , respectively, for all daytime SZA, unless SZA becomes $>90^\circ$ when, H' and β both increase stepwise with SZA (90° through 99°) with H' increasing from 74 to 87 km (at night), and β increasing from 0.3 to 0.5 km^{-1} (at night). H' and β then maintain these constant nighttime values of 87 and 0.5 km^{-1} , respectively, for all nighttime SZA.

This internal ("LWPM") ionospheric model was not used here because it is outdated. We used LWPC or ModeFinder only with user supplied (D region) ionospheric data (either as H' and β or as electron density vs. height profiles). LWPC has its own internal conductivity map and so is to be preferred over ModeFinder when there is significant low conductivity ground, particularly if this varies along the path, such as for NAA to St. John's here. LWPC may be preferable, on occasion, because it calculates the geomagnetic field parameters in each segment along the path. ModeFinder is also more suitable for comparing with loop antenna (i.e., magnetic field) observations on short (~ 300 km) paths (Thomson, 2010; see also Thomson et al. (2014, 2017). ModeFinder appears to be more stable at higher VLF/LF frequencies, appearing to be less likely to miss modes; it can also be simpler to use, particularly with electron density versus height profiles. Most of these issues were found to be not very significant for the accuracies required here.

LWPC was typically not needed (nor preferred to ModeFinder) for short paths or those that varied slowly along their lengths such as the terminator-aligned paths here. However, a mode-conversion code such as LWPC will definitely be required for calculations on paths across a dawn/dusk terminator, using our new rapidly changing (with SZA) path parameters shown in Figures 3 and 4, unless the path is very short (\sim few hundred km) or the path is aligned within a few degrees of the terminator.

6.4. Rocket Comparisons

Mechtly and Smith (1970) reported rocket observations near dawn at Wallops Island, Virginia, USA (38°N , 70°W). The electron number densities were measured as functions of height using a combination of probe currents and radio propagation (Faraday rotation together with differential absorption). Data from their dawn profile taken at SZA = 90° on 24 July 1968 is reproduced here in Figure 5 (green circles). Using this profile in ModeFinder for the NSY-Oakington path (as described above in Section 3.1) results in a calculated phase at the receiver of $-106^\circ \equiv 254^\circ$ (modulo 360°) which is 10° higher than the observed phase (at SZA = 90°) of 244° . When the rocket profile is raised by 2 km (shown with blue circles in Figure 5), the ModeFinder calculated phase at the receiver became $-120^\circ \equiv 240^\circ$, slightly lower (by 4°) than the observed phase. However the calculated amplitudes, 56.2 dB for the actual rocket profile and 59.3 dB for the raised profile, were significantly higher than the 54.3 dB actually observed. These higher amplitude are likely due to the rocket techniques not adequately measuring the electron densities below 60–65 km (e.g., Thomson et al., 2022).

As shown in our Figures 3 and 4, the VLF technique used here on the NSY-Cambridge path gives $H' = 72.75$ km and $\beta = 0.378\text{ km}^{-1}$ for SZA = -90.2° at dawn (and $H' = 72.2$ km and $\beta = 0.364\text{ km}^{-1}$ for SZA = -89.2°). Figure 5 shows, as the solid black line, the corresponding electron number densities from ModeFinder, using

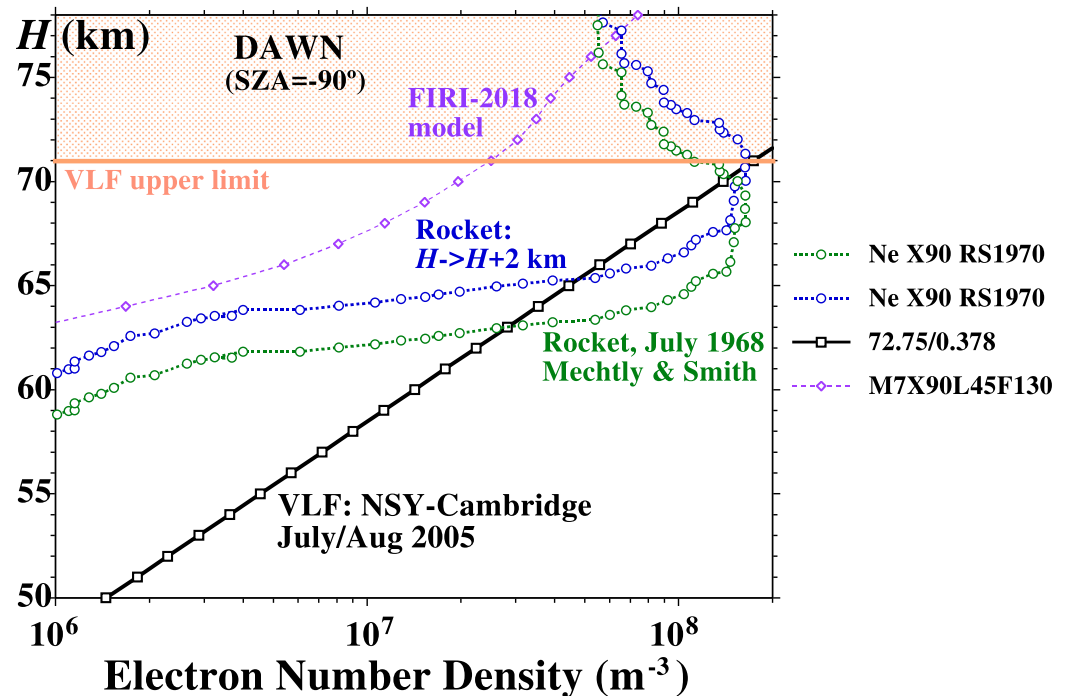


Figure 5. Electron number density height profiles at dawn (solar zenith angle (SZA) = -90°) at mid-latitude. The green circles are from the data, reported by Mechtly and Smith (1970), from a rocket flown at Wallops Island (38°N), Virginia, USA, on 24 July 1968. The blue circles are the same rocket data but raised in height by 2 km (see text). The heavy black line with square plot symbols is from the NSY-Cambridge very low frequency (VLF) path, 30 July–4 Aug 2005, where $H' = 72.75$ km and $\beta = 0.378$ km $^{-1}$ matched the data (at SZA = -90°). The orange line at 71 km is indicating the greatest height at which the VLF propagation on this path is sensitive to the electron number density. The purple diamonds are from the FIRI-2018 rocket-based model at dawn (SZA = -90°), for July at latitude 45° .

$H' = 72.75$ km and $\beta = 0.378$ km $^{-1}$, resulting in the observed amplitude of 54.3 dB and phase of -116° at the Cambridge receiver. Clearly this VLF profile matches well with the height of the Mechtly and Smith (1970) rocket profiles but has more electrons below ~ 60 km; these low altitude electrons are immersed in the higher density neutral atmosphere there and so have high (electron-neutral) collision frequencies, resulting in the higher VLF attenuation as actually observed. VLF propagation by day is generally not sensitive to electron densities above height, H' (e.g., Thomson et al., 2022, and references therein); in Figure 5 the orange line at 71 km is indicating the greatest height at which the VLF propagation on this NSY-Cambridge path was found here (using ModeFinder) to be sensitive to the electron number density.

Also shown in Figure 5 for further comparison is the rocket-derived FIRI-2018 (Friedrich et al., 2018) electron density profile for an SZA of 90° for July at 45° latitude (and solar activity F10.7 = 130 sfu though this is non-critical). As can be seen, the FIRI electron densities are somewhat lower than the others consistent with the comparisons of Thomson et al. (2022) who found generally good agreement between VLF-derived electron density profiles and FIRI-2018 at their common altitudes except at the lowest altitudes at (high) mid-latitudes, due to the lower sensitivity of the rocket technique at the lowest altitudes and the significant galactic cosmic ray generation of electrons there.

6.5. Early Ground-Based Radio Observations in the UK and Australia

Thomas and Harrison (1970) used VLF and LF measurements (typically reflection and polarization coefficients) recorded in the UK in the summer months of 1948–1950, together with full-wave calculations similar to those of Pitteway (1965) to calculate pre-sunrise electron density versus height profiles over a range of SZA ($>105^\circ$, 99° , 98° , 97° , 95° , 93° , 91.5° , and 90°). The first two of these profiles (SZA $>105^\circ$ and 99° , i.e., essentially nighttime) agree quite well with the much more recent nighttime rocket-based FIRI (Friedrich et al., 2018) and VLF-based profiles presented in Thomson et al. (2022). As the SZA decreases from 97° to 90° the Thomas and

Harrison (1970) profiles descend from ~ 80 to ~ 60 km with the peak electron densities increasing from $\sim 2 \times 10^7 \text{ m}^{-3}$ to $\sim 1.4 \times 10^8 \text{ m}^{-3}$ (at 65 km at 90°). To compare with our more recent results, their lowest profile (i.e., for $\text{SZA} = 90^\circ$) was entered into ModeFinder for our, similar-latitude, ~ 748 -km path, DHO (Germany) to Eskdalemuir (Scotland) resulting in 68.5 dB and 204° for the calculated amplitude and phase at the receiver. While the amplitude is quite similar to that actually observed, their profile phase of 204° is quite a lot higher than the $\sim 120^\circ$ actually observed (Figure S9 in Supporting Information S1) which means their dawn ($\text{SZA} = 90^\circ$) profile is likely to be too low in height (by ~ 4 km). Also, by comparing with our Figure 5 (where our H'/β profile for NSY-Oakington there is very similar to that for DHO-Eskdalemuir), it can be seen their electron density at ~ 65 km appears to be too high by a factor of ~ 3 . None-the-less their results are impressive for such early observations.

Smith et al. (1967) determined D region electron densities above Armidale, NSW, Australia (30.5°S , 151.5°E geographic, $\sim 36^\circ\text{S}$ geomagnetic) during ~ 1963 -65 using a medium frequency (~ 1 -2 MHz) pulsed cross-modulation technique, from night through dawn to mid-day. Their electron number densities from night to dawn ($\text{SZA} = -90^\circ$) are very broadly similar to, though somewhat less than, the UK values of Thomas and Harrison (1970). This is consistent with the Armidale results being at a lower geomagnetic latitude than those in the UK ($\sim 36^\circ$ vs. $\sim 55^\circ$), resulting in lower cosmic ray intensity there. The Armidale peak electron density at $\text{SZA} = -90^\circ$ (dawn) at a height of 65 km was $\sim 8 \times 10^7 \text{ m}^{-3}$, closer to our $\sim 7 \times 10^7 \text{ m}^{-3}$ (Figure 5, 65 km) than the UK value $\sim 14 \times 10^7 \text{ m}^{-3}$ of Thomas and Harrison (1970). When the ($\text{SZA} = -90^\circ$) Armidale electron densities are used in ModeFinder for our NSY-Oakington path, the predicted phase and amplitude, -107° and 55.2 dB, are fairly similar to the observed values, -117° and 54.4 dB. Most of the phase difference can be removed by raising the Armidale profile by just over 1 km, while the higher amplitude for the Armidale profile is probably due to it having too few electrons below ~ 60 km. However, the geomagnetic latitude of the mid-point of our NSY-Oakington path ($\sim 48^\circ\text{N}$) is somewhat higher than that of Armidale ($\sim 36^\circ\text{N}$). None-the-less the very broad agreement between these earlier (UK and Australian) observations and those reported here seems quite reasonable.

7. Summary and Conclusions

Characteristics of VLF radio propagation conditions near dawn and dusk in the lower D region (altitudes ~ 55 -90 km) of the Earth's ionosphere were determined using phases and amplitudes of subionospheric VLF radio waves. The VLF waves analysed propagated along either fairly short paths (~ 300 -1,000 km) or along paths which aligned with the dawn/dusk terminator (to keep the SZA fairly constant along the path). For most paths the phases and amplitudes observed at the receiver near (say) dawn (or dusk) were measured relative to those observed at mid-day on the same day; these differences were then added to the corresponding phase or amplitude calculated for mid-day from previously determined D region parameters to get dawn/dusk values independent of the phase or amplitude at the transmitter. Such mid-day calculations are likely to be more accurate at low latitudes or in summer (or at least, not in winter when the D region is more variable).

The VLF propagation conditions were characterized with the two "Wait" parameters, H' as a measure of the height and β as a measure of the sharpness (or slope) of the electron densities in the lower D region. The work reported here enabled these two parameters to be determined as functions of SZA in 3 latitude ranges: mid-latitudes, low latitudes and high mid-latitudes. For the first time these parameters have been able to be determined through dawn and dusk which should not only provide observational data for modeling the D region at these times but also extend the coverage range of VLF propagation monitoring for geophysical phenomena such as lightning, solar flares, and energetic particle precipitation.

The plots of H' and β against SZA also illustrate geophysical effects in the D region itself, including the greater role (and so SZA -dependence) of solar EUV (Lyman- α) at low and mid-latitudes and the greater role of GCR (and so SZA -independence) at increasingly higher mid-latitudes. In particular, the marked minimum observed in H' versus SZA at dawn at mid-latitudes (due to the release of cosmic ray generated electrons accumulated over night) reported here for the first time, shows how very different dawn propagation conditions are from dusk at mid-latitudes. Again, the observed absence of such a minimum at low latitudes emphasizes the reduced cosmic ray activity there compared with mid- and higher latitudes and also emphasizes that the dawn day-night transition in the D region is very different at low latitudes and mid-latitudes.

Data Availability Statement

The data underlying our VLF observations reported here are available at <http://doi.org/10.5281/zenodo.14210954> or (in some cases) from Thomson et al. (2007, 2012, 2014, 2017). The FIRI-2018 model profiles are available from <https://figshare.com/s/357cb03b3e5bed649bbc> (Friedrich et al., 2018) or <https://figshare.com/search?q=FIRI-2018>. US Navy code LWPC is available at <https://github.com/mlhutchins/LWPC>. The US Navy computer program referred to here as ModeFinder is a slightly modified version of MODEFNDR (e.g., Nunn & Strangeways, 2000; Thomson, 1993) and MODESRCH described and listed in Morfitt and Shellman (1976). Solar zenith angles were determined from NOAA's solar calculator at <https://gml.noaa.gov/grad/solcalc/>, or, often more conveniently and appropriately for this study, from their spreadsheets at (<https://gml.noaa.gov/grad/solcalc/calcdetails.html>). Geomagnetic latitudes came from the NOAA/NCEI World Magnetic Model: <https://www.ncei.noaa.gov/products/world-magnetic-model> specifically from: <https://www.ncei.noaa.gov/sites/default/files/2022-03/GeomagneticCoordinates.pdf>.

References

- Araki, T. (1973). Anomalous diurnal changes of transequatorial VLF radio waves. *Journal of Atmospheric and Terrestrial Physics*, 35(4), 693–703. [https://doi.org/10.1016/0021-9169\(73\)90200-6](https://doi.org/10.1016/0021-9169(73)90200-6)
- Araki, T., Kitayama, S., & Kato, S. (1969). Transequatorial reception of VLF radio waves from Australia. *Radio Science*, 4(4), 367–369. <https://doi.org/10.1029/RS004i004p0367>
- Banks, P. M., & Kockarts, G. (1973). *Aeronomy*. Academic.
- Barman, K., Das, B., Pal, S., Haldar, P. K., Midya, S. K., Pal, S., & Mondal, S. K. (2024). D-region ionospheric disturbances due to the December 2019 solar eclipse observed using multi-station VLF radio network. *Advances in Space Research*, 74(3), 1460–1470. <https://doi.org/10.1016/j.asr.2024.04.049>
- Basak, T., Hobara, Y., Pal, S., Nakamura, T., Izutsu, J., & Minatohara, T. (2024). Modeling of Solar Eclipse effects on the sub-ionospheric VLF/LF signals observed by multiple stations over Japan. *Advances in Space Research*, 73(1), 736–746. <https://doi.org/10.1016/j.asr.2023.09.063>
- Bilitza, D., Altadill, D., Truhlik, V., Shubin, V., Galkin, I., Reinisch, B., & Huang, X. (2017). International Reference Ionosphere 2016: From ionospheric climate to real-time weather predictions. *Space Weather*, 15(2), 418–429. <https://doi.org/10.1002/2016SW001593>
- Chand, A. E., & Kumar, S. (2017). VLF modal interference distance and night-time D region VLF reflection height for west-east and east-west propagation paths to Fiji. *Radio Science*, 52(8), 1004–1015. <https://doi.org/10.1002/2016RS006221>
- Chand, A. E., & Kumar, S. (2021). Earth-ionosphere waveguide model parameters using VLF transmissions received in the South Pacific region. *IEEE Access*, 9, 56653–56663. <https://doi.org/10.1109/ACCESS.2021.3072133>
- Cheng, Z., Cummer, S. A., Baker, D. N., & Kanekal, S. G. (2006). Nighttime D region electron density profiles and variabilities inferred from broadband measurements using VLF radio emissions from lightning. *Journal of Geophysical Research*, 111(A5). <https://doi.org/10.1029/2005JA011308>
- Chowdhury, S., Kundu, S., Basak, T., Ghosh, S., Hayakawa, M., Chakraborty, S., et al. (2021). Numerical simulation of lower ionospheric reflection parameters by using International Reference Ionosphere (IRI) model and validation with Very Low Frequency (VLF) radio signal characteristics. *Advances in Space Research*, 67(5), 1599–1611. <https://doi.org/10.1016/j.asr.2020.12.017>
- Clilverd, M. A., Rodger, C. J., Gamble, R. J., Ulich, T., Raita, T., Seppälä, A., et al. (2010). Ground-based estimates of outer radiation belt energetic electron precipitation fluxes into the atmosphere. *Journal of Geophysical Research*, 115(A12). <https://doi.org/10.1029/2010JA015638>
- Clilverd, M. A., Rodger, C. J., Thomson, N. R., Brundell, J. B., Ulich, T., Lichtenberger, J., et al. (2009). Remote sensing space weather events: Antarctic-arctic radiation-belt (dynamic) deposition-VLF atmospheric Research Consortium network. *Space Weather*, 7(4), S04001. <https://doi.org/10.1029/2008SW000412>
- Clilverd, M. A., Rodger, C. J., van de Kamp, M., & Verronen, P. T. (2020). Electron precipitation from the outer radiation belt during the St. Patrick's day storm 2015: Observations, modeling, and validation. *Journal of Geophysical Research: Space Physics*, 125(2). <https://doi.org/10.1029/2019JA027725>
- Clilverd, M. A., Smith, A. J., & Thomson, N. R. (1991). The annual variation in quiet time plasmaspheric electron density, determined from whistler mode group delays. *Planetary and Space Science*, 39(7), 1059–1067. [https://doi.org/10.1016/0032-0633\(91\)90113-O](https://doi.org/10.1016/0032-0633(91)90113-O)
- Crombie, D. D. (1964). Periodic fading of VLF signals received over long paths during sunrise and sunset. *Radio Science Journal of Research NBS/USNC-URSI*, 68D(1), 27–34. <https://doi.org/10.6028/jres.068D.012>
- Cummer, S. A., Inan, U. S., & Bell, T. F. (1998). Ionospheric D region remote sensing using VLF radio atmospherics. *Radio Science*, 33(6), 1781–1792. <https://doi.org/10.1029/98RS02381>
- Ferguson, J. A. (1998). *Computer programs for assessment of long-wavelength radio communications, version 2.0: User's guide and source files*. SPAWAR Technical Document 3030. Space and Naval Warfare Systems Center. Retrieved from <https://apps.dtic.mil/sti/pdfs/ADA350375.pdf>
- Ferguson, J. A., & Snyder, F. P. (1990). *Computer programs for assessment of long wavelength radio communications, version 1.0: Full FORTRAN code user's guide*. Naval Ocean Systems Center Tech. Doc. 1773, DTIC AD-B144 839, Defence Technical Information Center.
- Fishman, G. J., & Inan, U. S. (1988). Observation of an ionospheric disturbance caused by a gamma-ray burst. *Nature*, 331(6155), 418–420. <https://doi.org/10.1038/331418a0>
- Friedrich, M., Pock, C., & Torkar, K. (2018). FIRI-2018, an updated empirical model of the lower ionosphere. *Journal of Geophysical Research: Space Physics*, 123(8), 6737–6751. <https://doi.org/10.1029/2018JA025437>
- Funke, B., Dudok de Wit, T., Ermolli, I., Haberreiter, M., Kinnison, D., Marsh, D., et al. (2024). Towards the definition of a solar forcing dataset for CMIP7. *Geoscientific Model Development*, 17(3), 1217–1227. <https://doi.org/10.5194/gmd-17-1217-2024>
- Han, F., & Cummer, S. A. (2010). Midlatitude daytime D region ionosphere variations measured from radio atmospherics. *Journal of Geophysical Research*, 115(A10). <https://doi.org/10.1029/2010JA015715>
- Heaps, M. G. (1978). Parameterization of the cosmic ray ion-pair production rate above 18 km. *Planetary and Space Science*, 26(6), 513–517. [https://doi.org/10.1016/0032-0633\(78\)90041-7](https://doi.org/10.1016/0032-0633(78)90041-7)

Acknowledgments

Many of the VLF observations used here were supported by funding from the UK Research and Innovation (UKRI-NERC) through National Capability–Space Weather Observatory.

- ITU-R. (2015). *International telecommunications union, radio communications sector, recommendation ITU-R P.832-4, world atlas of ground conductivities*. P-series, Radiowave Propagation. Retrieved from https://www.itu.int/dms_pubrec/itu-r/rec/p/R-REC-P.832-4-201507-1!!PDF-E.pdf
- Koh, K., Bennett, A., Ghilain, S., Liu, Z., Pedeboy, S., Peverell, A., & Füllekrug, M. (2019). Lower ionospheric conductivity modification above a thunderstorm updraught. *Journal of Geophysical Research: Space Physics*, *124*(8), 6938–6949. <https://doi.org/10.1029/2019JA026863>
- Kumar, A., & Kumar, S. (2020). Ionospheric D region parameters obtained using VLF measurements in the South Pacific region. *Journal of Geophysical Research: Space Physics*, *125*(1), e2019JA027536. <https://doi.org/10.1029/2019JA027536>
- Macotela, E. L., Clilverd, M., Renkowitz, T., Chau, J., Manninen, J., & Baniś, D. (2021). Spring-fall asymmetry in VLF amplitudes recorded in the North Atlantic region: The fall-effect. *Geophysical Research Letters*, *48*(16), e2021GL094581. <https://doi.org/10.1029/2021GL094581>
- Macotela, E. L., Clilverd, M. A., Manninen, J., Thomson, N. R., Newnham, D. A., & Raita, T. (2019). The effect of ozone shadowing on the D region ionosphere during sunrise. *Journal of Geophysical Research*, *124*(5), 3729–3742. <https://doi.org/10.1029/2018JA026415>
- Matthes, K., Funke, B., Andersson, M. E., Barnard, L., Beer, J., Charbonneau, P., et al. (2017). Solar forcing for CMIP6 (v3.2). *Geoscientific Model Development*, *10*(6), 2247–2302. <https://doi.org/10.5194/gmd-10-2247-2017>
- McCormick, J. C., & Cohen, M. B. (2021). A new four-parameter D-region ionospheric model: Inferences from lightning-emitted VLF signals. *Journal of Geophysical Research: Space Physics*, *126*(12), e2021JA029849. <https://doi.org/10.1029/2021JA029849>
- Mechtly, E. A., & Smith, L. G. (1970). Changes of lower ionosphere electron densities with solar zenith angle. *Radio Science*, *5*(12), 1407–1412. <https://doi.org/10.1029/RS005i012p01407>
- Morfitt, D. G., & Shellman, C. H. (1976). “MODESRCH”, an improved computer program for obtaining ELF/VLF/LF mode constants in an Earth/ionosphere waveguide (naval electr. Lab. Cent. Interim rep. 77T, NTIS accession ADA032573). National Technical Information Service. Retrieved from <https://apps.dtic.mil/sti/pdfs/ADA032573.pdf>
- Morgan, R. R. (1968). Westinghouse world-wide VLF conductivity map. AD0675771. <https://apps.dtic.mil/sti/pdfs/AD0675771.pdf>
- Neal, J. J., Rodger, C. J., Clilverd, M. A., Thomson, N. R., Raita, T., & Ulich, T. (2015). Long-term determination of energetic electron precipitation into the atmosphere from ARDDVARK subionospheric VLF observations. *Journal of Geophysical Research*, *120*(3), 2194–2211. <https://doi.org/10.1002/2014JA020689>
- Neher, H. V., & Anderson, H. R. (1962). Cosmic rays at balloon altitudes and the solar cycle. *Journal of Geophysical Research*, *67*(4), 1309–1315. <https://doi.org/10.1029/JZ067i004p01309>
- Nunn, D., & Strangeways, H. J. (2000). Trimperturbations from large ionisation enhancement patches (LIEs). *Journal of Atmospheric and Terrestrial Physics*, *62*(3), 189–206. [https://doi.org/10.1016/S1364-6826\(00\)00004-3](https://doi.org/10.1016/S1364-6826(00)00004-3)
- Pal, S., Hobar, Y., Shvets, A., Schnoor, P. W., Hayakawa, M., & Koloskov, O. (2023). First detection of global ionospheric disturbances associated with the most powerful gamma ray burst GRB221009A. *Atmosphere*, *14*(2), 217. <https://doi.org/10.3390/atmos14020217>
- Pappert, R. A., & Snyder, F. P. (1972). Some results of a mode-conversion program for VLF. *Radio Science*, *7*(10), 913–923. <https://doi.org/10.1029/RS007i010p00913>
- Peterson, J. R. (1976). Sunlight photodestruction of CO₃⁻, CO₃⁻-H₂O, and O₃⁻: The importance of photodissociation to the D region electron densities at sunrise. *Journal of Geophysical Research*, *81*(7), 1433–1435. <https://doi.org/10.1029/JA081i007p01433>
- Pitteway, M. L. V. (1965). The numerical calculation of wave-fields, reflection coefficients and polarizations for long radio waves in the lower ionosphere. I., *Philosophical Transactions of the Royal Society*, *A257*(1079), 219–241. <https://doi.org/10.1098/rsta.1965.0004>
- Reid, G. C. (1976). Ion chemistry in the D region. In D. R. Bates & B. Bederson (Eds.), *Ion chemistry in the D region. Advances in atomic and molecular physics* (Vol. 12, pp. 375–413). Academic Press. [https://doi.org/10.1016/S0065-2199\(08\)60047-0](https://doi.org/10.1016/S0065-2199(08)60047-0)
- Reid, G. C. (1987). Radar observations of negative-ion photodetachment at sunrise in the auroral-zone mesosphere. *Planetary and Space Science*, *35*(1), 27–37. [https://doi.org/10.1016/0032-0633\(87\)90141-3](https://doi.org/10.1016/0032-0633(87)90141-3)
- Rodger, C. J., Brundell, J. B., & Dowden, R. L. (2005). Location accuracy of VLF world wide Lightning Location (WWLL) network: Post-algorithm upgrade. *Annales Geophysicae*, *23*(2), 277–290. <https://doi.org/10.5194/angeo-23-277-2005>
- Rodger, C. J., Clilverd, M. A., Seppälä, A., Thomson, N. R., Gamble, R. J., Parrot, M., et al. (2010). Radiation belt electron precipitation due to geomagnetic storms: Significance to middle atmosphere ozone chemistry. *Journal of Geophysical Research*, *115*, A11. <https://doi.org/10.1029/2010JA015599>
- Rozhnoi, A., Solovieva, M., Shalimov, S., Ouzounov, D., Gallagher, P., Verth, G., et al. (2020). The effect of the 21 August 2017 total solar eclipse on the phase of VLF/LF signals. *Earth and Space Science*, *7*(2), e2019EA000839. <https://doi.org/10.1029/2019EA000839>
- Said, R. K., Inan, U. S., & Cummins, K. L. (2010). Long-range lightning geolocation using a VLF radio atmospheric waveform bank. *Journal of Geophysical Research*, *115*, D23. <https://doi.org/10.1029/2010JD013863>
- Sechrist, C. F. (1968). Interpretation of pre-sunrise electron densities and negative ions in the D-region. *Journal of Atmospheric and Terrestrial Physics*, *30*(3), 371–389. [https://doi.org/10.1016/0021-9169\(68\)90109-8](https://doi.org/10.1016/0021-9169(68)90109-8)
- Smith, R. A., Coyne, T. N. R., Loch, R. G., & Bourne, I. A. (1967). Small perturbation wave interaction in the lower ionosphere, 3, measurements of electron densities, ground-based radio wave propagation studies of the lower ionosphere 1. In J. S. Belrose, I. A. Bourne, & L. W. Hewitt (Eds.), *Defence Research telecommunications establishment* (pp. 335–358). Retrieved from https://publications.gc.ca/collections/collection_2019/isde-ised/DR50-2-1967-1-eng.pdf
- Thomas, L., & Bowman, M. R. (1986). A study of pre-sunrise changes in negative ions and electrons in the D-region. *Annales Geophysicae, Series A*, *4*(3), 219–227.
- Thomas, L., & Harrison, M. D. (1970). The electron density distributions in the D-region during the night and pre-sunrise period. *Journal of Atmospheric and Terrestrial Physics*, *32*(1), 1–14. [https://doi.org/10.1016/0021-9169\(70\)90158-3](https://doi.org/10.1016/0021-9169(70)90158-3)
- Thomson, N. R. (1993). Experimental daytime VLF ionospheric parameters. *Journal of Atmospheric and Terrestrial Physics*, *55*(2), 173–184. [https://doi.org/10.1016/0021-9169\(93\)90122-F](https://doi.org/10.1016/0021-9169(93)90122-F)
- Thomson, N. R. (2010). Daytime tropical D region parameters from short path VLF phase and amplitude. *Journal of Geophysical Research*, *115*(A9). <https://doi.org/10.1029/2010JA015355>
- Thomson, N. R., & Clilverd, M. A. (2001). Solar flare induced ionospheric D-region enhancements from VLF amplitude observations. *Journal of Atmospheric and Terrestrial Physics*, *63*(16), 1729–1737. [https://doi.org/10.1016/S1364-6826\(01\)00048-7](https://doi.org/10.1016/S1364-6826(01)00048-7)
- Thomson, N. R., Clilverd, M. A., & McRae, W. M. (2007). Nighttime ionospheric D region parameters from VLF phase and amplitude. *Journal of Geophysical Research*, *112*(A7). <https://doi.org/10.1029/2007JA012271>
- Thomson, N. R., Clilverd, M. A., & Rodger, C. J. (2011). Daytime midlatitude D region parameters at solar minimum from short-path VLF phase and amplitude. *Journal of Geophysical Research*, *116*(A3). <https://doi.org/10.1029/2010JA016248>

- Thomson, N. R., Clilverd, M. A., & Rodger, C. J. (2014). Low-latitude ionospheric *D* region dependence on solar zenith angle. *Journal of Geophysical Research: Space Physics*, *119*(8), 6865–6875. <https://doi.org/10.1002/2014JA020299>
- Thomson, N. R., Clilverd, M. A., & Rodger, C. J. (2017). Midlatitude ionospheric *D* region: Height, sharpness, and solar zenith angle. *Journal of Geophysical Research: Space Physics*, *122*(8), 8933–8946. <https://doi.org/10.1002/2017JA024455>
- Thomson, N. R., Clilverd, M. A., & Rodger, C. J. (2018). Quiet daytime Arctic ionospheric *D* region. *Journal of Geophysical Research: Space Physics*, *123*(11), 9726–9742. <https://doi.org/10.1029/2018JA025669>
- Thomson, N. R., Clilverd, M. A., & Rodger, C. J. (2022). Ionospheric *D* region: VLF-measured electron densities compared with rocket-based FIRI-2018 model. *Journal of Geophysical Research: Space Physics*, *127*(11), e2022JA030977. <https://doi.org/10.1029/2022JA030977>
- Thomson, N. R., & McRae, W. M. (2009). Nighttime ionospheric *D* region: Equatorial and non-equatorial. *Journal of Geophysical Research*, *114*(A8). <https://doi.org/10.1029/2008JA014001>
- Thomson, N. R., Rodger, C. J., & Clilverd, M. A. (2005). Large solar flares and their ionospheric *D* region enhancements. *Journal of Geophysical Research*, *110*(A6). <https://doi.org/10.1029/2005JA011008>
- Thomson, N. R., Rodger, C. J., & Clilverd, M. A. (2011b). Daytime *D* region parameters from long-path VLF phase and amplitude. *Journal of Geophysical Research*, *116*(A11). <https://doi.org/10.1029/2011JA016910>
- Thomson, N. R., Rodger, C. J., & Clilverd, M. A. (2012). Tropical daytime lower *D* region dependence on sunspot number. *Journal of Geophysical Research*, *117*(A10). <https://doi.org/10.1029/2012JA018077>
- Verronen, P. T., Ulich, T., Turunen, E., & Rodger, C. J. (2006). Sunset transition of negative charge in the *D*-region ionosphere during high-ionization conditions. *Annales Geophysicae*, *24*(1), 187–202. <https://doi.org/10.5194/angeo-24-187-2006>
- Wait, J. R., & Spies, K. P. (1964). *Characteristics of the Earth-ionosphere waveguide for VLF radio waves*. NBS Tech. Natl. Bur. of Stand. Retrieved from <https://www.govinfo.gov/app/details/GOVPUB-C13-1fc83a916d87542f34917847f89b9f0b>
- Worthington, E. R., & Cohen, M. B. (2021). The estimation of *D*-region electron densities from trans-ionospheric very low frequency signals. *Journal of Geophysical Research: Space Physics*, *126*(6), e2021JA029256. <https://doi.org/10.1029/2021JA029256>
- Xu, W., Marshall, R. A., Bortnik, J., & Bonnell, J. W. (2021). An electron density model of the *D*- and *E*-region ionosphere for transionospheric VLF propagation. *Journal of Geophysical Research: Space Physics*, *126*(7), e2021JA029288. <https://doi.org/10.1029/2021JA029288>
- Zhou, X., Wang, J., Ma, D., Huang, Q., & Xiao, F. (2021). A method for determining *D* region ionosphere reflection height from lightning skywaves. *Journal of Atmospheric and Solar-Terrestrial Physics*, *221*, 105692. <https://doi.org/10.1016/j.jastp.2021.105692>